Available online at www.sciencedirect.com
SCIENCE DIRECT®
Journal of Sound and Vibration 281 (2005) 719–741
JOURNAL OF SOUND AND VIBRATION
www.elsevier.com/locate/jsvi

The forced vibration of an elastic plate under significant fluid loading

C.J. Chapman[a,*], S.V. Sorokin[b]

[a]*Department of Mathematics, University of Keele, Keele, Staffordshire ST5 5BG, UK*
[b]*Department of Engineering Mechanics, State Marine Technical University, Lotsmanskaya Street 3, Saint Petersburg 190008, Russia*

Received 18 September 2003; accepted 2 February 2004
Available online 3 September 2004

Abstract

This paper gives an asymptotic analysis of the sound and vibration produced when a metal plate, which could be part of the hull of a ship, is forced into motion by its contact with vibrating machinery on one side, and radiates sound into water on the other side. The frequency range is that for which the water significantly affects the vibration of the plate. The mathematical method used is scaling of the frequency with the square of the intrinsic fluid-loading parameter to maximise the number of terms in the dispersion relation which balance at leading order. This 'significant' scaling, which gives accurate results over a wide frequency range, is used to obtain scaling laws for all aspects of the acoustic field and plate vibration, including the sizes of the different parts of the near field, the amount of radiated acoustic energy, and the amount of energy propagating in the surface wave. The results extend a previous asymptotic theory of heavy fluid loading, valid only in a restricted part of the frequency range covered by significant loading.

1. Introduction

This work concerns the classical problem of a metal plate forced into motion by its contact with vibrating machinery on one side, and radiating sound into a fluid, taken to be water, on the other

*Corresponding author. Tel.: +44-1782-583-262; fax: +44-1782-584-268.
E-mail address: c.j.chapman@maths.keele.ac.uk (C.J. Chapman).

0022-460X/$ - see front matter © 2005 Elsevier Ltd. All rights reserved.
doi:10.1016/j.jsv.2004.02.013

side. The metal plate might be part of the hull of a ship. The frequency range to be considered is that for which, in the surface wave which propagates along the plate and in the neighbouring fluid, the inertia of both the fluid and the plate need to be taken into account. Thus, the fluid loading is heavy enough to affect significantly the magnitude and phase speed of the surface wave, but not so heavy that the inertia of the plate is negligible. Accordingly, the frequency range produces neither light nor heavy fluid loading, but significant fluid loading [1]. This frequency range is of considerable importance in practice. For example, a steel plate, of thickness 2 cm, with water on one side, is in the regime of significant fluid loading for a very wide range of frequencies around 200 Hz. Nevertheless, the literature does not contain a systematic account, with the emphasis on orders of magnitude and scaling laws, of results obtainable for the forced vibration of a plate under significant fluid loading. Even so comprehensive a writer on fluid loading as D.G. Crighton, who clearly identified the regime of significant fluid loading, nevertheless gave results only for light fluid loading and heavy fluid loading (e.g. Refs. [1,2]).

The effects of greatest interest in the problem are the sound field radiated directly into the fluid from the forcing region, and the surface wave propagating in the plate and neighbouring fluid. These effects are analysed in detail, both with regard to their numerical values and also the way in which these numerical values are determined by scaling laws. In particular, the scaling law for the energy flow in the surface wave is of fundamental importance in practice, since this energy flow, enormously greater than that in the directly radiated sound field, is available for conversion into sound at plate junctions and at inhomogeneities, e.g. at struts.

The basic variables in the problem are reducible to the dimensionless frequency Ω, the dimensionless wavenumber K, and the intrinsic fluid-loading parameter ε, also dimensionless, defined by

$$\Omega = \frac{\omega h/c_B}{(c_0/c_B)^2}, \quad K = \frac{kh}{c_0/c_B}, \quad \varepsilon = \frac{\rho_0/\rho}{c_0/c_B}. \tag{1}$$

Here ω is the frequency, k is the wavenumber, h is the thickness of the plate, ρ_0 is the density of the fluid, ρ is the density of the plate, c_0 is the sound speed of the fluid, and c_B is the bending-wave characteristic speed defined by the equation $E' = \rho c_B^2$, where $E' = E/\{12(1-\nu^2)\}$ and E, ν are Young's modulus and Poisson's ratio of the plate. The parameter ε, a coupling parameter between the fluid and plate, was defined originally by Gutin [3] and independently by Nayak [4]. For steel in water, $\rho_0/\rho \simeq 0.128$, $c_0/c_B \simeq 0.952$, and $\varepsilon \simeq 0.134$. In his series of papers on fluid-loading problems, culminating in the 1988 Rayleigh medal lecture and a textbook exposition, Crighton [1,2,5] came to advocate the systematic use of ε in perturbation expansions, not only because of its convenient smallness but also because of its independence of frequency. Thus, regimes may be identified by the powers of ε to which they correspond.

As observed by Crighton [1], and as elucidated below in Section 3.1, the regime in which Ω is of order ε^2 is special, in that the maximum possible number of terms in the dispersion relation then have the same order of magnitude in ε and can be balanced at leading order. This maximum number of terms is four, and the balanced terms correspond to plate stiffness, plate inertia, fluid inertia, and fluid pressure at the surface of the plate, so that the only negligible physical quantity is the fluid compressibility. Such a regime, in which a power of a small parameter has been selected to balance as many terms in an equation as possible at leading order, is called a significant regime (or distinguished regime, or preferred regime). For a significant regime, truncated series expansions in a

small parameter are far more accurate, and have a far wider range of validity, than they do for a non-significant regime. This is only to be expected, because a significant regime retains the maximum number of physical processes for which an expansion in a small parameter is possible. In this paper, the regime in which Ω is of order ε^2 is called the regime of significant fluid loading. As noted earlier, the regime is of considerable importance in practice, i.e. the four physical quantities retained are indeed important simultaneously in a practically important frequency range.

The above remarks show that it is natural to define a reduced frequency Ω_0 by $\Omega = \Omega_0\varepsilon^2$, so that significant fluid loading corresponds formally to Ω_0 of order one. Then significant fluid loading problems may be analysed by means of expansions in powers of ε at fixed Ω_0. Note from (Eq. 1) that

$$\Omega_0 = \frac{\omega h/c_B}{(\rho_0/\rho)^2}. \tag{2}$$

Thus the reduced frequency Ω_0 is independent of c_0, the speed of sound in the fluid, corresponding to the fact that, for significant loading, the fluid in the surface wave is effectively incompressible, i.e. has negligible potential energy. Heavy loading corresponds to $\Omega \ll \varepsilon^2$, i.e. $\Omega_0 \ll 1$, or 'low frequency', and light loading corresponds to $\Omega \gg \varepsilon^2$, i.e. $\Omega_0 \gg 1$, or 'high frequency'. In heavy loading, the physical quantities retained at leading order are plate stiffness, fluid inertia, and pressure at the plate surface; i.e. plate inertia has become negligible. In light loading, the leading order quantities are plate stiffness and plate inertia only; i.e. the fluid motion and pressure have become 'slaves' to the motion of the plate.

In the literature, the term 'fluid loading parameter' is used in different senses, for example to refer to $\Omega_0^{-1/2}$ or Ω_0^{-1} in the notation used here. In either sense, significant fluid loading corresponds to an order-one value of this fluid loading parameter, and heavy fluid loading corresponds to a high value of this parameter. The key idea exploited in the present paper is that even when this parameter is of order one, a perturbation series approach is still available and valuable because of the smallness of the intrinsic fluid loading parameter ε. Another use of the term fluid loading parameter has been to mean $1/(\varepsilon\Omega_0)$. Unfortunately, this use does not correspond to a rational scaling, as the effect of fluid loading on the plate vibration is negligible when $\varepsilon\Omega_0$ is of order one.

The structure of the paper is as follows. In Section 2, the governing equations for forced vibration are solved for the velocity potential, acoustic pressure, and plate displacement, and the solution is expressed in a form ideal for numerical computation. Typical numerical results are presented. The rest of the paper derives scaling laws: in Section 3 for the dispersion relation and its zeros; in Section 4 for the surface wave, especially its pressure field, plate displacement, and energy flow; in Section 5 for the acoustic field, including its energy flow and the energy budget for the whole problem; and in Section 6 for the inner near field. Conclusions are presented in Section 7.

2. Governing equations and their solution

2.1. Governing equations

A stationary compressible fluid of density ρ_0 and sound speed c_0 occupies the half-space $y > 0$ in a Cartesian coordinate system (x, y, z). The boundary of the half-space is a thin elastic plate of

density (per unit volume) ρ, Young's modulus E, Poisson's ratio v, and thickness h; the plate occupies the layer $-h<y<0$. The half-space $y<-h$ contains fluid of negligible density compared with ρ_0, which is ignored henceforth. The lower surface $y=-h$ of the plate is forced by a pressure distribution independent of z, but otherwise an arbitrary function of time t and position x, denoted $f(t,x)$. The geometry of the problem, in the dimensionless variables defined below in the last paragraph of Section 2.2, is shown in Fig. 1. The acoustic velocity of the fluid is $\mathbf{u}=(u,v,0)$, representable by a potential $\phi(t,x,y)$ as $\mathbf{u}=\nabla\phi$, so that, with subscripts denoting differentiation, $u=\phi_x$ and $v=\phi_y$. The acoustic pressure p in the fluid is $p=-\rho_0\phi_t$.

The displacement $\eta(t,x)$ of the plate is assumed to satisfy the bending-wave equation [6, pp. 236–239, 250–255]; [7, pp. 17–20, 253–257]. This equation has coefficients depending on ρ, h, and the bending-wave characteristic speed c_B defined in Section 1. The boundary-value problem to be solved is

$$c_0^{-2}\phi_{tt}-\phi_{xx}-\phi_{yy}=0 \quad (y>0), \tag{3}$$

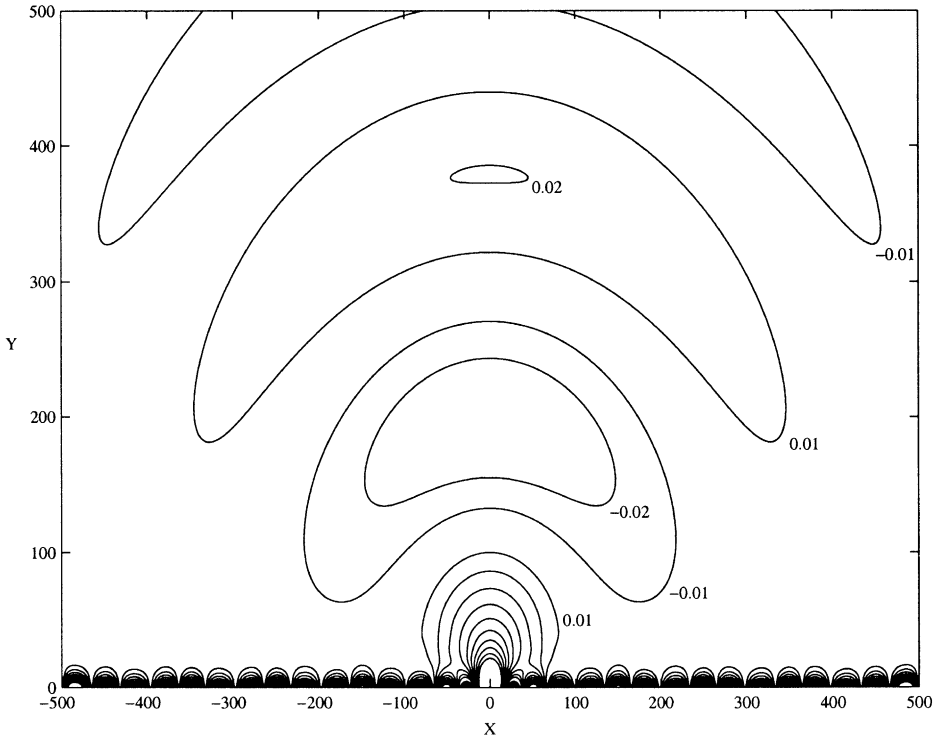

Fig. 1. Contours of the real part of the scaled acoustic pressure P, satisfying Eqs. (19)–(20), for $\varepsilon=0.134$ and $\Omega_0=1$, i.e. $\Omega=0.0180$; thus the frequency is 0.0180 of the coincidence frequency $\omega_c=(c_0/c_B)^2c_B/h$. Contour levels of P are from ±0.01 to ±0.1 in steps of 0.01. The radius of the acoustic near-field scales with the wavelength of the acoustic wave radiating into the fluid; embedded in this near field is a much smaller inner near field, which scales with the wavelength of the surface wave, propagating next to the plate. In the original dimensional variables, these wavelengths are of order c_0/ω and $(\rho_0/\rho)(c_B/\omega)$, the latter independent of c_0; in scaled dimensionless variables, used in the plot, the wavelengths are of order ε^{-2} and ε^{-1}.

$$\rho h\eta_{tt} + \rho c_B^2 h^3 \eta_{xxxx} = \rho_0 \phi_t + f(t,x) \quad (y=0), \tag{4}$$

$$\eta_t = \phi_y \quad (y=0). \tag{5}$$

Here $\rho_0\phi_t$ is the coupling between the fluid and the plate, i.e. $-p(t,x,0)$. The approximate boundary condition (5) represents continuity of velocity normal to the mean plate boundary $y=0$; similarly, in (4) the forcing $f(t,x)$ is placed on this boundary $y=0$ rather than on $y=-h$. Eqs. (3)–(5) will later be supplemented by radiation and causality conditions. Differentiation of (Eq. 4) with respect to t, followed by substitution of $\eta_t = \phi_y$ from (Eq. 5), gives the boundary condition on $y=0$ in terms of ϕ alone as

$$\rho_0\phi_{tt} - \rho h\phi_{tty} - \rho c_B^2 h^3 \phi_{xxxxy} = -f_t \quad (y=0). \tag{6}$$

2.2. Velocity potential

Eqs. (3)–(6) may be solved for ϕ by taking Fourier transforms in t and x. Frequency is represented by ω, and wavenumber conjugate to x by k. Fourier transforms, represented by capital letters, are defined according to the convention

$$\Phi = \Phi(\omega,k,y) = \int_{-\infty}^{\infty}\int_{-\infty}^{\infty} \phi(t,x,y) \mathrm{e}^{\mathrm{i}(\omega t - kx)}\,\mathrm{d}x\,\mathrm{d}t, \tag{7}$$

$$\phi = \phi(t,x,y) = \frac{1}{4\pi^2}\int_{-\infty}^{\infty}\int_{-\infty}^{\infty} \Phi(\omega,k,y) \mathrm{e}^{-\mathrm{i}(\omega t - kx)}\,\mathrm{d}k\,\mathrm{d}\omega. \tag{8}$$

For ϕ to represent a causal solution to (3)–(6), the ω contour in the inversion integral (8) must lie above all singularities in the complex ω plane. Real and imaginary parts of a complex variable are denoted by subscripts r and i, so that, for example, $\omega = \omega_\mathrm{r} + \mathrm{i}\omega_\mathrm{i}$. The variables t, x, and y are always real.

Subsequent formulae involve the complex quantity γ defined in terms of the complex variables ω and k by $\gamma = \gamma(\omega,k) = (k^2 - (\omega/c_0)^2)^{1/2}$. The branch of the square root is chosen so that $\gamma_\mathrm{r} > 0$ when k is real and ω_i is small and positive. The Fourier transform of the wave equation (3) is $\Phi_{yy} - \gamma^2\Phi = 0$. Since Φ cannot grow exponentially as $y \to \infty$, the relevant solution of this equation is proportional to $\mathrm{e}^{-\gamma y}$. The solution Φ may thus be written in terms of a function $A(\omega,k)$ as $\Phi = A(\omega,k)\mathrm{e}^{-\gamma y}$. If the Fourier transform of $f(t,x)$ is denoted $F(\omega,k)$, the Fourier transform of the boundary condition (6) gives

$$A(\omega,k) = \frac{-\mathrm{i}\omega F(\omega,k)}{\rho_0\omega^2 + (\rho h\omega^2 - \rho c_B^2 h^3 k^4)\gamma(\omega,k)}. \tag{9}$$

Hence (Eq. 8) gives

$$\phi = -\frac{\mathrm{i}}{4\pi^2}\int_{-\infty}^{\infty}\int_{-\infty}^{\infty} \frac{\omega F(\omega,k)\mathrm{e}^{-\mathrm{i}(\omega t - kx) - \gamma(\omega,k)y}}{\rho_0\omega^2 + (\rho h\omega^2 - \rho c_B^2 h^3 k^4)\gamma(\omega,k)}\,\mathrm{d}k\,\mathrm{d}\omega. \tag{10}$$

Ambiguities arising from poles on a real contour of integration are resolved by giving ω in the integrand a small positive imaginary part. Differentiation of (Eq. 10) with respect to (t,x,y)

corresponds to multiplication of the integrand by $(-\mathrm{i}\omega, \mathrm{i}k, -\gamma)$; and reciprocally for integration. Thus, (p, u, v, η) are obtained from (Eq. 10) by multiplying F by $(\mathrm{i}\rho_0\omega, \mathrm{i}k, -\gamma, -\mathrm{i}\omega^{-1}\gamma)$, the last of these evaluated on $y = 0$.

The dimensionless frequency Ω, the dimensionless wavenumber K, and the intrinsic fluid loading parameter ε were defined in (Eq. 1). In terms of the coincidence frequency ω_c and the coincidence wavenumber k_c, defined by

$$\omega_c = (c_0/c_B)^2 c_B/h, \quad k_c = (c_0/c_B)/h, \tag{11a, b}$$

the dimensional frequency and wavenumber are $\omega = \omega_c\Omega$, $k = k_cK$. The dimensionless version of γ is $\Gamma = (K^2 - \Omega^2)^{1/2}$, so that $\gamma = k_c\Gamma$. Dimensionless time T and lengths X, Y are $T = \omega_c t$ and $X = k_c x$, $Y = k_c y$. Then by (Eq. 10) the potential ϕ is

$$\phi = -\frac{\mathrm{i}}{4\pi^2}\frac{1}{\rho h}\int_{-\infty}^{\infty}\int_{-\infty}^{\infty}\frac{\Omega F(\omega_c\Omega, k_cK)\mathrm{e}^{-\mathrm{i}(\Omega T - KX) - \Gamma(\Omega,K)Y}}{\varepsilon\Omega^2 + (\Omega^2 - K^4)(K^2 - \Omega^2)^{1/2}}\,\mathrm{d}K\,\mathrm{d}\Omega. \tag{12}$$

A steel plate of thickness 2 cm in water has $\omega_c = 7.14 \times 10^4\,\mathrm{rad\,s^{-1}}$ and $k_c = 47.6\,\mathrm{rad\,m^{-1}}$, corresponding to 11.4 kHz and wavelength 13.2 cm. Thus frequencies of interest in practice are much less than ω_c; and indeed the simple bending-wave equation (4) becomes invalid as the coincidence frequency is approached.

2.3. Pressure

The acoustic pressure p is obtained from the potential ϕ as described after (Eq. 10), i.e. by multiplying F by $\mathrm{i}\rho_0\omega$. It is convenient henceforth to use polar coordinates (R, θ) defined by $(X, Y) = (R\cos\theta, R\sin\theta)$, and to change the wavenumber variable of integration K to an angle χ, which may be complex, defined as a root of $K = \Omega\cos\chi$. The root is chosen by specifying a contour of integration in the χ plane and taking $\Gamma = (K^2 - \Omega^2)^{1/2} = -\mathrm{i}\Omega\sin\chi$. The resulting contour, called a Sommerfeld contour, is of a type widely used in wave theory and in Bessel-function asymptotics; see, for example, Figs. 5.7 and 6.7 in [8, pp. 238, 267], and Figs. 5.13 and 5.14 in [9, pp. 623, 630], together with their accompanying text. Use of χ eliminates branch points and branch lines from all integrals; i.e. χ is a natural coordinate for specifying position on the two-sheeted Riemann surface covering the K plane. Thus the acoustic pressure is

$$p = -\frac{1}{4\pi^2}\frac{\rho_0 c_0^2}{\rho c_B h^2}\int_{-\infty}^{\infty}\Omega\mathrm{e}^{-\mathrm{i}\Omega T}\int_C\frac{F(\omega_c\Omega, k_c\Omega\cos\chi)}{D(\varepsilon,\Omega,\chi)}\mathrm{e}^{\mathrm{i}\Omega R\cos(\theta-\chi)}\sin\chi\,\mathrm{d}\chi\,\mathrm{d}\Omega, \tag{13}$$

where

$$D(\varepsilon,\Omega,\chi) = \varepsilon - \mathrm{i}\Omega(1 - \Omega^2\cos^4\chi)\sin\chi. \tag{14}$$

The roots χ of the dispersion relation $D(\varepsilon, \Omega, \chi) = 0$ give poles in the integrand of (Eq. 13). In the strip of interest in the χ plane, consisting of all χ for which $-\frac{1}{2}\pi \leqslant \chi_{\mathrm{r}} < \frac{3}{2}\pi$, there are ten poles, because the dispersion relation is a quintic in $\sin\chi$, and each of the five roots $\sin\chi$ gives two values of χ. In Fig. 2 the five poles in the upper half of the χ plane are labelled $\chi_{u1}, \ldots, \chi_{u5}$, and the five poles in the lower half of the χ plane are labelled $\chi_{l1}, \ldots, \chi_{l5}$. The numbering is chosen to increase from left to right. If the Ω integration in (Eq. 13) is performed last, the allowed χ contours C

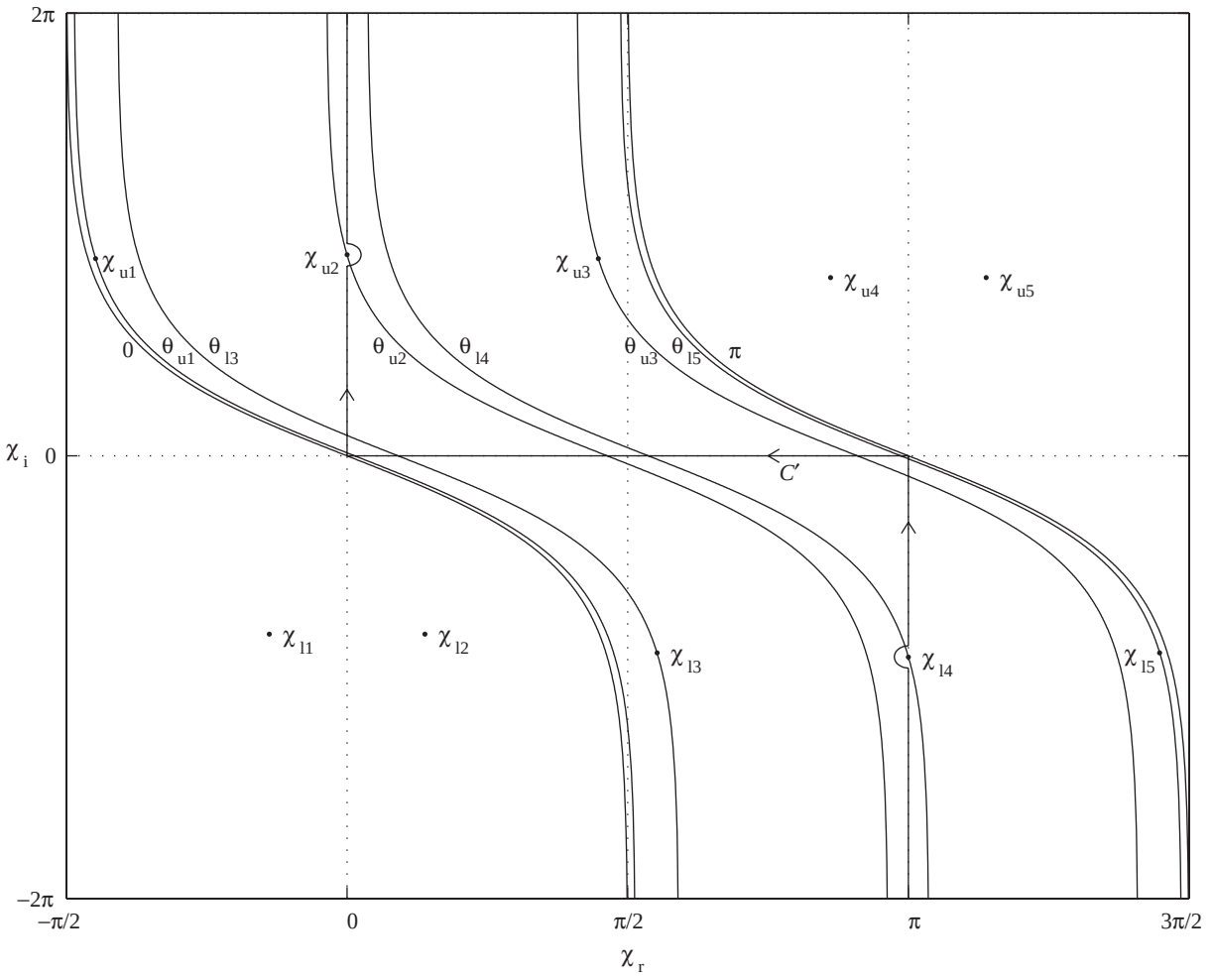

Fig. 2. Poles $\chi = \chi_{u1}, \ldots, \chi_{l5}$ in contour integrals with respect to χ, for $\varepsilon = 0.134$ and $\Omega_0 = 1$, i.e. $\Omega = 0.0180$; the poles are the roots χ of the dispersion relation $D(\varepsilon, \Omega, \chi) = 0$. For each observation angle θ there is a saddle point on the real χ axis at $\chi = \theta$, and a corresponding steepest-descent path through $\chi = \theta$. The curves labelled $\theta_{u1}, \ldots, \theta_{l5}$ are the steepest-descent paths which pass through the poles $\chi = \chi_{u1}, \ldots, \chi_{l5}$, corresponding to saddle points on the real χ-axis at $\chi = \theta_{u1}, \ldots, \theta_{l5}$. The curves labelled $0, \pi$ are the steepest-descent paths for $\theta = 0, \pi$. The original contour of integration is C', indented as shown around the poles χ_{u2}, χ_{l4}.

depend on Ω. The Ω contour lies above all singularities in the Ω plane. When Ω is real and positive, the simplest allowed χ contour is that marked C' in Fig. 1; this contour runs from $\pi - i\infty$ to $i\infty$ and is piecewise linear, except for an indentation to the right around the pole χ_{u2}, which always lies on $\chi_r = 0$, and an indentation to the left around the pole χ_{l4}, which always lies on $\chi_r = \pi$. The contour C' corresponds in the K plane to the indented real K-axis. Contours for other values of Ω are obtained by analytic continuation from C', as described in Ref. [10]. For example, when Ω is real and negative, the simplest allowed contour is the reflection of C' about the line

$\chi_r = \frac{1}{2}\pi$; the dispersion relation $D(\varepsilon, \Omega, \chi) = 0$ implies that if Ω is real then a change to $-\Omega$ transforms the poles to their complex conjugates.

The term $e^{i\Omega R\cos(\theta-\chi)}$ in the χ integral in (Eq. 13) has a saddle point at $\chi = \theta$, through which runs a steepest-descent path in the χ plane. For the moment it will be assumed that Ω is real and positive, so that the steepest-descent path does not depend on Ω and may be denoted $C(\theta)$. The extension to other Ω is straightforward. The equation of $C(\theta)$ is $\cos(\theta - \chi_r)\cosh\chi_i = 1$, i.e.

$$\chi_i = \mathrm{sgn}(\theta - \chi_r)\cosh^{-1}(\sec(\theta - \chi_r)) \quad (\theta - \tfrac{1}{2}\pi < \chi_r < \theta + \tfrac{1}{2}\pi) \tag{15}$$

or

$$\chi_r = \theta - \mathrm{sgn}(\chi_i)\cos^{-1}(\mathrm{sech}\,\chi_i) \quad (-\infty < \chi_i < \infty). \tag{16}$$

Here $\cosh^{-1}$ and $\cos^{-1}$ indicate principal values. Variation of θ translates $C(\theta)$ horizontally in the χ plane. The path $C(\theta)$ extends from $\chi = \theta + \frac{1}{2}\pi - i\infty$ to $\chi = \theta - \frac{1}{2}\pi + i\infty$, as shown in Fig. 2, which gives plots of $C(\theta)$ for several values of θ.

An extremely rapid numerical method of evaluating the χ integral in (Eq. 13) is to deform the original contour C' on to the steepest-descent contour $C(\theta)$. Then the value of the integral is the sum of (i) residue contributions from poles crossed in the deformation; and (ii) the contour integral over $C(\theta)$. For example, in Fig. 2 the deformation of C' onto $C(0)$ crosses, in order, the poles $\chi_{u2}, \chi_{l3}, \chi_{u1}$; and similarly, the deformation of C' onto $C(\pi)$ crosses the poles $\chi_{l4}, \chi_{u3}, \chi_{l5}$. Numerical evaluation of the contour integral is almost instantaneous because of the decay of the integrand away from $\chi = \theta$. Evaluation of the residue contributions requires a method for determining, as a function of θ, the poles which are crossed between C' and $C(\theta)$. Such a method is the following. Let $\theta(\chi)$ denote the value of θ for which the steepest-descent path $C(\theta)$ passes through the point χ. Thus $\theta(\chi)$ is a real-valued function defined in the χ plane; its level lines are the curves $C(\theta)$. By (Eq. 16),

$$\theta(\chi) = \chi_r + \mathrm{sgn}(\chi_i)\cos^{-1}(\mathrm{sech}\,\chi_i). \tag{17}$$

The ten poles $\chi_{u1}, \ldots, \chi_{l5}$ determine ten angles $\theta(\chi_{u1}), \ldots, \theta(\chi_{l5})$, which will be denoted $\theta_{u1}, \ldots, \theta_{l5}$. Symmetries are $\theta_{l5} = \pi - \theta_{u1}$, $\theta_{l4} = \pi - \theta_{u2}$, etc. As θ varies from 0 to π, the poles are cut on or cut off at those angles $\theta_{u1}, \ldots, \theta_{l5}$ which lie in the range 0 to π. Thus in a numerical code the cut on/cut off is accounted for by multiplying each residue contribution by plus or minus a Heaviside unit step function with argument plus or minus $\theta - \theta_{u1}, \ldots$; the signs are determined from Fig. 2 by the fact that $\chi_{u1}, \chi_{u2}, \chi_{l1}, \chi_{l2}, \chi_{l3}$ lie to the left of the original contour C', whereas $\chi_{u3}, \chi_{u4}, \chi_{u5}, \chi_{l4}, \chi_{l5}$ lie to the right.

For definiteness, attention will henceforth be confined to point forcing at a fixed frequency. Thus in terms of a reference pressure p_0, a reference length a, and an arbitrary real positive frequency ω', the forcing pressure on the plate is taken to be $f(t, x) = p_0\delta(x/a)e^{-i\omega' t}$. Then, $F(\omega, k) = 2\pi a p_0 \delta(\omega - \omega')$, so that, with $\omega' = \omega_c\Omega'$,

$$F(\omega_c\Omega, k_c\Omega\cos\chi) = 2\pi a p_0 \omega_c^{-1}\delta(\Omega - \Omega'). \tag{18}$$

Evaluation of the Ω integral in (Eq. 13), followed by dropping of the dash on Ω', and then expression in terms of the reduced frequency Ω_0 by means of $\Omega = \varepsilon^2\Omega_0$, gives the acoustic pressure

in the form

$$p = \frac{\rho_0}{\rho}\frac{a}{h} p_0 \mathrm{e}^{-\mathrm{i}\varepsilon^2\Omega_0 T} P, \tag{19}$$

where

$$P = P(\varepsilon, \Omega_0, R, \theta) = -\frac{\varepsilon\Omega_0}{2\pi}\int_{C'} \frac{\mathrm{e}^{\mathrm{i}\varepsilon^2\Omega_0 R\cos(\theta-\chi)}}{D_0(\varepsilon,\Omega_0,\chi)}\sin\chi\,\mathrm{d}\chi \tag{20}$$

and

$$D_0(\varepsilon,\Omega_0,\chi) = 1 - \mathrm{i}\varepsilon\Omega_0(1-\varepsilon^4\Omega_0^2\cos^4\chi)\sin\chi. \tag{21}$$

It is convenient to refer to P as 'the pressure,' since by (Eq. 19) it gives a dimensionless form of p when T is zero or a multiple of $2\pi/(\varepsilon^2\Omega_0)$. Deformation of C' on to the steepest-descent contour $C = C(\theta)$, as just described, decomposes P into a contribution from poles, P_{poles}, and a contribution from the steepest-descent integral, P_{steep}. Thus

$$P = P_{\text{poles}} + P_{\text{steep}}. \tag{22}$$

In numerical evaluation of P_{steep}, the variable of integration may be taken to be χ_{r}. On $C(\theta)$, (Eq. 15) gives

$$\chi = \chi_{\text{r}} + \mathrm{i}\,\mathrm{sgn}(\theta-\chi_{\text{r}})\cosh^{-1}(\sec(\theta-\chi_{\text{r}})), \quad \mathrm{d}\chi = (1 - \mathrm{i}\,\sec(\theta-\chi_{\text{r}}))\,\mathrm{d}\chi_{\text{r}}, \tag{23a, b}$$

so that

$$P_{\text{steep}} = \frac{\varepsilon\Omega_0}{2\pi}\int_{\theta-(1/2)\pi}^{\theta+(1/2)\pi} \frac{\mathrm{e}^{\mathrm{i}\varepsilon^2\Omega_0 R\cos(\theta-\chi)}}{D_0(\varepsilon,\Omega_0,\chi)}\sin\chi\,(1-\mathrm{i}\,\sec(\theta-\chi_{\text{r}}))\,\mathrm{d}\chi_{\text{r}}. \tag{24}$$

Here χ is the function of χ_{r} given by Eq. (23a), and the sign change between Eqs. (20) and (24) occurs because the direction of C' is from $\theta+\frac{1}{2}\pi$ to $\theta-\frac{1}{2}\pi$. Other useful ways of writing the integral for P_{steep} are given in Appendix A.

Numerical evaluation of P_{poles} and P_{steep}, and hence of P, was performed as described above for many values of ε and Ω_0, and the results were examined as contour plots of the real and imaginary parts P_{r} and P_{i} in the (X, Y) plane. A typical result is shown in Fig. 1, which gives a contour plot of P_{r} for $\varepsilon = 0.134$ and $\Omega_0 = 1$, i.e. $\Omega = 0.0180$. Thus, the frequency is 0.0180 of the coincidence frequency $\omega_c = (c_0/c_B)^2 c_B/h$. The figure shows vividly the large-amplitude surface wave propagating near the plate away from the forcing point $(X, Y) = (0, 0)$, and the much smaller amplitude sound wave propagating into the fluid away from this point. The surface wave propagating to the right, i.e. for $X>0$, is described by the contribution to P_{poles} from the pole $\chi = \chi_{u2}$; the surface wave propagating to the left, i.e. for $X<0$, is described by the contribution from the pole $\chi = \chi_{l4}$; and the sound wave, including its near field (but excluding the inner near field), is described by P_{steep}. The sound field outside of the near field, i.e. for R greater than about 100 in the figure, is described by the saddle-point approximation to P_{steep}, for which the saddle point is at $\chi = \theta$. The inner near field, i.e. the region where R is less than about 10 in the figure, requires for its description not only P_{steep} without approximation but also the contribution to P_{poles} from the surface-wave poles χ_{u2}, χ_{l4} and the evanescent-wave poles $\chi_{u1}, \chi_{u3}, \chi_{l3}, \chi_{l5}$. Thus in the frequency range of interest the only quantities which nowhere affect the field are the 'irrelevant

poles' $\chi_{u4}, \chi_{u5}, \chi_{l1}, \chi_{l2}$, lying well outside the curved strip of the χ plane swept by the steepest-descent contours $C(\theta)$ for $0 \leqslant \theta \leqslant \pi$.

2.4. Plate displacement

The plate displacement η is obtained from the velocity potential φ as described after (Eq. 10), i.e. by multiplying $F(\omega, k)$ by $-\mathrm{i}\omega^{-1}\gamma(\omega, k)$ and evaluating the resulting integral corresponding to (Eq. 10) on $y = 0$, i.e. on $\theta = 0, \pi$. For the single-frequency forcing introduced in Section 2.3, this gives

$$\eta = \frac{p_0}{\rho_0 c_0^2} \frac{c_B}{c_0} a \mathrm{e}^{-\mathrm{i}\varepsilon^2 \Omega_0 T} W, \tag{25}$$

where

$$W = W(\varepsilon, \Omega_0, R, \theta) = -\frac{\mathrm{i}}{2\pi\varepsilon} \int_{C'} \frac{\mathrm{e}^{\mathrm{i}\varepsilon^2 \Omega_0 R \cos(\theta - \chi)}}{D_0(\varepsilon, \Omega_0, \chi)} \sin^2 \chi \, \mathrm{d}\chi \quad (\theta = 0, \pi). \tag{26}$$

For convenience, W will also be referred to as the displacement. Expression (26) extended to the range $0 < \theta < \pi$ gives the analytical continuation of W above the X-axis; although this continuation is not needed, the use of (R, θ) instead of X is helpful in making the formulae similar to those for the pressure. Thus as before, the contour C' is deformed onto the steepest-descent contour $C(\theta)$, to give a decomposition of W into a contribution from poles, W_{poles}, and a contribution from the steepest-descent integral, W_{steep}. Hence,

$$W = W_{\text{poles}} + W_{\text{steep}}. \tag{27}$$

Analogously to (Eq. 24),

$$W_{\text{steep}} = -\frac{\mathrm{i}}{2\pi\varepsilon} \int_{\theta-(1/2)\pi}^{\theta+(1/2)\pi} \frac{\mathrm{e}^{\mathrm{i}\varepsilon^2 \Omega_0 R \cos(\theta - \chi)}}{D_0(\varepsilon, \Omega_0, \chi)} \sin^2 \chi \, (1 - \mathrm{i} \sec(\theta - \chi_{\mathrm{r}})) \, \mathrm{d}\chi_{\mathrm{r}} \quad (\theta = 0, \pi), \tag{28}$$

where χ is the function of χ_{r} given by Eq. (23a). Numerical evaluation of W_{poles} and W_{steep}, and hence of W, are rapidly performed as described in Section 2.3.

2.5. Numerical calculation and scaling laws

From a numerical point of view, the problem set in Section 2.1 may be regarded as completely solved. The pressure field, the plate displacement, and all other dependent variables are rapidly computed by the method above. However, the main aim of this paper is to give scaling laws, in the frequency range of significant fluid loading, to explain and expand upon the numerical results. For example, a quantity of great practical importance is the energy flux in the surface wave, since this energy flux, far greater than the acoustic energy radiated directly from the forcing region, is available for scattering into sound at inhomogeneities and struts in the plate. A basic task is to determine the power of ε in the leading term of a series expansion of each needed quantity, for example P_{poles} and P_{steep}, and to provide a method of calculating the order-one factor which multiplies this power of ε. The dependence of the important quantities, e.g. the above energy flux,

on the many parameters in the problem is readily obtained. Accordingly, the scaling of all formulae will now be determined. A scaling aspect already apparent in Fig. 1 is the disparity between the small wavelength of the surface wave and the large wavelength of the radiated sound; their ratio is of order ε.

3. Dispersion relation, scalings, and poles

3.1. The dispersion relation and its scaling

In dimensionless variables (Ω, K), the dispersion relation for problem (3)–(5) is

$$\varepsilon\Omega^2 + (\Omega^2 - K^4)(K^2 - \Omega^2)^{1/2} = 0. \tag{29}$$

This is obtained by equating to zero the denominator of the integrand in (Eq. 12). The most important consequence of (Eq. 29) is the dependence on ε and Ω of its roots K in the complex plane. A perturbation approach will be adopted, since $\varepsilon \ll 1$ in applications. The first stage is to find the dominant balances: thus, the exponents (m, n) in an assumed scaling $\Omega \sim \varepsilon^m$, $K \sim \varepsilon^n$ are chosen so that at leading order the maximum number of terms in (Eq. 29) have the same order of magnitude. This gives $(m, n) = (2, 1), (0, 0)$. Expansions based on $(m, n) = (0, 0)$ become non-uniform when (Ω, K) approach the coincidence values $(1, 1)$; hence, a further dominant balance exists of the form $\Omega - 1 \sim \varepsilon^r$, $K - 1 \sim \varepsilon^s$. This gives $(r, s) = (\frac{2}{3}, \frac{2}{3})$. Balances of these three types, but with the emphasis on membranes rather than plates, were first identified in Ref. [11]. As discussed in Section 1, a scaling based on a leading-order balance of the maximum possible number of terms in an equation is called a significant scaling (or distinguished scaling, or preferred scaling), and leads to approximations accurate over a far wider range of parameter values than approximations based on a non-significant scaling. Moreover, all results arising from a non-significant scaling are obtainable from a significant scaling by taking an appropriate limit, but not vice versa.

This paper is concerned only with the balance $(m, n) = (2, 1)$, i.e. $\Omega \sim \varepsilon^2$, $K \sim \varepsilon$, since, as stated above, applications relate to $\Omega \ll 1$. A suitable expansion of solutions of the dispersion relation (29) is

$$\Omega = \varepsilon^2\Omega_0, \quad K = \varepsilon K_0 + \varepsilon^3 K_1 + \cdots . \tag{30a, b}$$

Here Ω_0 is the reduced frequency, as defined in Section 1. From (Eq. 30b), it is natural to define a reduced wavenumber by $1\ K/\varepsilon$, which by (Eq. 1) is $kh/(\rho_0/\rho)$ in dimensional variables. Solutions of the dispersion relation for significant fluid loading have their reduced wavenumber of order one and are approximately independent of the speed of sound c_0 in the fluid. In (Eq. 30a,b) and henceforth, subscripted variables such as Ω_0, K_0, K_1 (and later χ_1, χ_2) are dimensionless and of order one. Thus, the order of magnitude of all calculated quantities, such as pressure, displacement, and energy flow, is evident from the leading power of ε, and numerical detail is provided by the order-one relationships between Ω_0, K_0, K_1, etc. The primary task of this paper is to provide this numerical detail by calculating the dependence of all quantities on the reduced

frequency Ω_0. Thus, substitution of (Eq. 30a,b) into (Eq. 29) and collection of powers of ε leads to

$$K_0^5 - \Omega_0^2 K_0 \mp \Omega_0^2 = 0, \quad K_1 = \pm \frac{\Omega_0^2}{2K_0(4K_0 \pm 5)}. \tag{31a, b}$$

Eq. (31a) determines ten roots K_0 as functions of Ω_0; then Eq. (31b) gives the ten corresponding values of K_1 as functions of Ω_0. Both square roots in (Eq. 29) are allowed, in order to encompass the whole of the Riemann surface for K, and the relevant roots of Eq. (31a) are selected when the contour of integration is deformed. The relationship of Eqs. (30a,b), (31) to the heavy fluid loading limit is discussed in Appendix B.

In the variables Ω, χ, the dispersion relation may be written $D(\varepsilon, \Omega, \chi) = 0$, with the dispersion function $D(\varepsilon, \Omega, \chi)$ given by (Eq. 14). When $\Omega = \varepsilon^2 \Omega_0$, it is convenient to use the scaled dispersion function $D_0(\varepsilon, \Omega_0, \chi)$ defined by $D = \varepsilon D_0$, so that $D_0(\varepsilon, \Omega_0, \chi)$ is given by (Eq. 21) and the dispersion relation is equivalent to $D_0(\varepsilon, \Omega_0, \chi) = 0$. Since $\cos\chi = K/\Omega$, expansion (30a,b) shows that the roots χ of the dispersion relation satisfy $\cos\chi \simeq \varepsilon^{-1} K_0/\Omega_0$. Hence, $\chi = \pm \mathrm{i}\,\ln(2\varepsilon^{-1} K_0/\Omega_0) + \mathrm{O}(\varepsilon^2)$, so that $\chi_\mathrm{i} \simeq \pm\ln(\varepsilon^{-1})$ and χ_r is of order one. The sign of χ_i will be indicated by means of the indicator variable $\sigma \equiv \mathrm{sgn}(\chi_\mathrm{i}) = \pm 1$. Then a suitable expansion of solutions of the dispersion relation is

$$\chi = \mathrm{i}\sigma \ln(\varepsilon^{-1}) + \chi_0 + \varepsilon^2 \chi_2 + \cdots . \tag{32}$$

Substitution of (Eq. 32) into the dispersion relation $D_0(\varepsilon, \Omega_0, \chi) = 0$, or transformation of Eq. (31), gives

$$\Omega_0^3 \mathrm{e}^{-5\mathrm{i}\sigma\chi_0} - 16\Omega_0 \mathrm{e}^{-\mathrm{i}\sigma\chi_0} - 32\sigma = 0, \quad \chi_2 = \mathrm{i}\sigma \mathrm{e}^{-2\mathrm{i}\sigma\chi_0} \frac{1 + \frac{3}{16}\Omega_0^2 \mathrm{e}^{-4\mathrm{i}\sigma\chi_0}}{1 - \frac{5}{16}\Omega_0^2 \mathrm{e}^{-4\mathrm{i}\sigma\chi_0}}. \tag{33a, b}$$

It is shown in Appendix B that the limit $\Omega_0 \ll 1$ leads to the non-significant approximation $K_0^5 \simeq \pm\Omega_0^2$. The corresponding approximation obtained from Eq. (33) is $\mathrm{e}^{-5\mathrm{i}\sigma\chi_0} \simeq 32\sigma\Omega_0^{-3}$ because $\mathrm{e}^{-\mathrm{i}\sigma\chi_0} = 2K_0/\Omega_0$.

3.2. Poles

In the vertical strip $-\frac{1}{2}\pi \leqslant \chi_\mathrm{r} < \frac{3}{2}\pi$, Eqs. (32)–(33) determine ten values of χ, five for $\sigma = 1$, i.e. $\chi_\mathrm{i} > 0$, and five for $\sigma = -1$, i.e. $\chi_\mathrm{i} < 0$. These are the poles $\chi_{u1}, \ldots, \chi_{u5}$ and $\chi_{l1}, \ldots, \chi_{l5}$ defined in Section 2.3 and shown in Fig. 2 for $\varepsilon = 0.134$, $\Omega_0 = 1$. On the scale of Fig. 2, the approximate positions $\mathrm{i}\sigma\ln(\varepsilon^{-1}) + \chi_0$ with χ_0 from Eq. (33a) are indistinguishable from the exact positions obtained from $D(\varepsilon, \Omega, \chi) = 0$. The symmetry of this equation, or of $D_0(\varepsilon, \Omega_0, \chi) = 0$, is discussed in Appendix C.

Tracks of the poles as Ω increases from 0.0002 to 2, i.e. as Ω_0 increases from 0.0111 to 111, are shown in Fig. 3. The coincidence frequency $\Omega = 1$ corresponds to $\Omega_0 = 55.8$. If the exact positions of the poles shown in Fig. 3 are compared with the approximate positions $\mathrm{i}\sigma\ln(1/\varepsilon) + \chi_0$, where χ_0 is obtained from Eq. (33a), it is found that Eq. (33a) locates the important poles $\chi_{u1}, \chi_{u2}, \chi_{u3}, \chi_{l3}, \chi_{l4}, \chi_{l5}$ accurately for frequencies up to about $\Omega = 0.5$, i.e. $\Omega_0 = 27.8$. Thus the significant approximation is useful remarkably close to the coincidence frequency, even though formally it is introduced for much lower frequencies. This is the usual situation when a significant approximation is used. The six important poles $\chi_{u1}, \ldots, \chi_{l5}$ in Fig. 3 move smoothly towards the

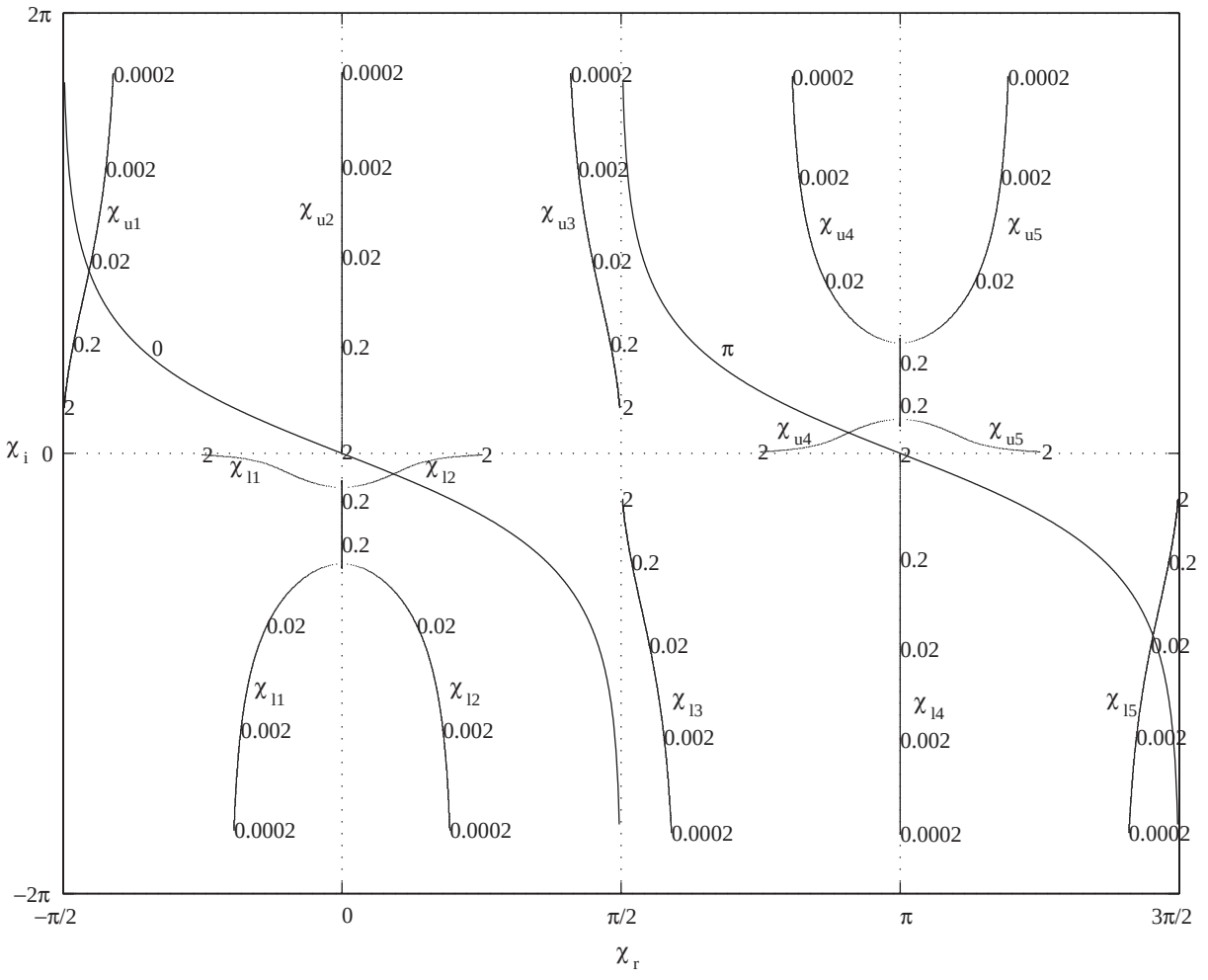

Fig. 3. Tracks of the poles $\chi = \chi_{u1}, \ldots, \chi_{l5}$ for $\varepsilon = 0.134$ as Ω varies from 0.0002 to 2, i.e. as Ω_0 varies from 0.0111 to 111; cf. Fig. 2 for $\Omega = 0.0180$, i.e. $\Omega_0 = 1$. The poles χ_{u1}, χ_{l5} cross the steepest-descent curves for $\theta = 0, \pi$ when $\Omega = 0.0258$, i.e. $\Omega_0 = 1.436$.

real axis as Ω_0 increases. The unimportant poles χ_{u4}, χ_{u5} coalesce on the line $\chi_r = \pi$ when $\Omega_0 = 4.2$, and they remain on this line, but distinct, until $\Omega_0 = 33$, when they coalesce again and leave the line on opposite sides, and similarly for the unimportant poles χ_{l1}, χ_{l2} in relation to the imaginary axis $\chi_r = 0$. The poles χ_{u4}, χ_{u5}, χ_{l1},χ_{l2} are not relevant to this paper, because in the frequency range of interest they are not crossed during deformations of the contour of integration, and are not close to the saddle point of the integrand.

Series expansions for $\theta = \theta_{u1}, \ldots, \theta_{l5}$, at which the poles cut on or cut off, are obtained by substituting into Eq. (17) expansion (32) for the poles. The result is

$$\theta = \tfrac{1}{2}\pi\sigma + \chi_{0r} - 2\sigma\varepsilon e^{-\sigma\chi_{0i}} + \varepsilon^2\chi_{2r} + \cdots . \tag{34}$$

Here χ_0, χ_2 satisfy Eq. (33), i.e. correspond to any of the ten poles; for each pole, Eq. (34) gives a function of Ω_0. The dependence of $\theta = \theta_{u1}, \ldots, \theta_{l5}$ on Ω in the range $0.002 \leqslant \Omega \leqslant 2$, i.e. $0.111 \leqslant \Omega_0 \leqslant 111$, is plotted in Fig. 4, obtained by substituting the roots χ of the dispersion relation $D(\varepsilon, \Omega, \chi) = 0$ into Eq. (17). If the exact curves shown in Fig. 4 are compared with the approximate curves $\frac{1}{2}\pi\sigma + \chi_{0r} - 2\sigma\varepsilon e^{-\sigma\chi_{0i}}$, where χ_0 is obtained from Eq. (33a), it is found that the approximations to the important curves $\theta_{u1}, \theta_{u2}, \theta_{u3}, \theta_{l3}, \theta_{l4}, \theta_{l5}$ are accurate for frequencies up to about $\Omega = 0.5$, i.e. $\Omega_0 = 27.8$. The curves in Fig. 4 may be checked against the tracks of $\chi_{u1}, \ldots, \chi_{l5}$ in Fig. 3. At $\Omega_0 = 1.436$, i.e. $\Omega = 0.0258$, calculation shows that $\theta_{u1} = 0$ and $\theta_{l5} = \pi$, i.e. χ_{u1} is on $C(0)$ and χ_{l5} is on $C(\pi)$. In the parameter range of interest in this paper, i.e. $\Omega = \Omega_0\varepsilon^2$ with $\varepsilon = 0.134$ and Ω_0 of order one, the above results imply that for $\Omega_0 > 1.436$ the poles χ_{u1}, χ_{l5} are not cut on for any θ in the relevant range $0 \leqslant \theta \leqslant \pi$.

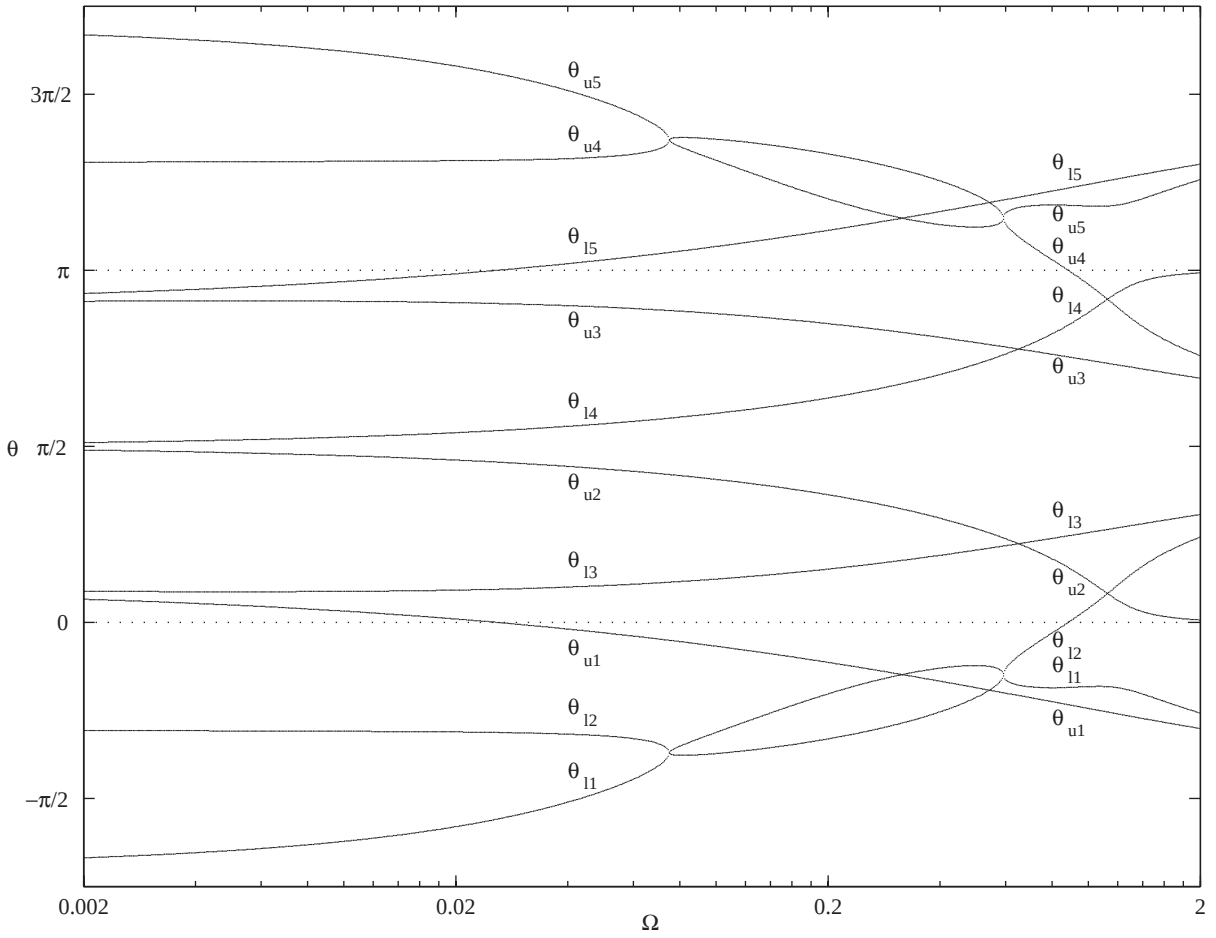

Fig. 4. Observation angles $\theta_{u1}, \ldots, \theta_{l5}$ at which the poles cut on or cut off, i.e. at which the steepest-descent paths pass through the poles $\chi_{u1}, \ldots, \chi_{l5}$. The figure is for $\varepsilon = 0.134$ and Ω from 0.002 to 2, i.e. Ω_0 from 0.111 to 111; cf. Figs. 2 and 3. At $\Omega = 0.0258$, i.e. $\Omega_0 = 1.436$, the curves θ_{u1}, θ_{l5} pass through the values $0, \pi$, i.e. χ_{u1} is then on $C(0)$, and χ_{l5} is on $C(\pi)$.

4. The surface wave

4.1. Pressure field in the surface wave

The surface wave travelling to the right in Fig. 1 is represented by the pole χ_{u2} in Fig. 2. The contribution of this pole to the pressure P will be denoted P_{u2}. It will now be shown that

$$P_{u2} \simeq -\frac{\mathrm{i}\Omega_0 \mathrm{e}^{(1/2)\varepsilon\Omega_0(-Y+\mathrm{i}X)\mathrm{e}^{\chi_{0\mathrm{i}}}}}{2(2\Omega_0+5\mathrm{e}^{-\chi_{0\mathrm{i}}})} H(\theta_{u2}-\theta), \tag{35}$$

where

$$\theta_{u2} = \tfrac{1}{2}\pi - 2\varepsilon \mathrm{e}^{-\chi_{0\mathrm{i}}} + O(\varepsilon^3) \tag{36}$$

and H denotes the Heaviside step function, which takes the value 0 for negative argument and 1 for positive argument. In formulae such as Eqs. (35)–(36) for pole contributions, quantities based on the variable χ are always assumed to be evaluated at the appropriate pole. Thus $\chi_{0\mathrm{i}}$ is a function of Ω_0 only, determined by Eq. (33a) with $\sigma = 1$. Since the pole $\chi = \chi_{u2}$ is on the imaginary axis, expansion (32)–(33) is applied with $\chi_{\mathrm{r}} = 0$, $\chi_{0\mathrm{r}} = 0$, $\chi_{2\mathrm{r}} = 0, \ldots$, i.e. $\chi = \mathrm{i}\chi_{\mathrm{i}}$, $\chi_0 = \mathrm{i}\chi_{0\mathrm{i}}$, $\chi_2 = \mathrm{i}\chi_{2\mathrm{i}}, \ldots$.

Expression (35) for P_{u2} is obtained from integral (20) for P as follows. Let P^+ denote the contribution to Eq. (20) from a small circuit around a pole χ, where the superscript + indicates that the circuit is taken anti-clockwise. Residue calculus gives

$$P^+ = -\mathrm{i}\varepsilon\Omega_0 \frac{\mathrm{e}^{\mathrm{i}\varepsilon^2\Omega_0 R\cos(\theta-\chi)}}{D_0'(\varepsilon,\Omega_0,\chi)} \sin\chi. \tag{37}$$

Here the dash on D_0' indicates differentiation with respect to χ, so that from Eq. (21),

$$D_0'(\varepsilon,\Omega_0,\chi) = -\mathrm{i}\varepsilon\Omega_0\{1-\varepsilon^4\Omega_0^2(1-6\sin^2\chi+5\sin^4\chi)\}\cos\chi. \tag{38}$$

The terms in Eq. (37) may be expanded in powers of ε by means of Eq. (32). Thus

$$\sin\chi = \tfrac{1}{2}\mathrm{i}\sigma\varepsilon^{-1}\mathrm{e}^{-\mathrm{i}\sigma\chi_0}\{1-\varepsilon^2(\mathrm{e}^{2\mathrm{i}\sigma\chi_0}+\mathrm{i}\sigma\chi_2)+O(\varepsilon^4)\}, \tag{39}$$

$$\cos\chi = \tfrac{1}{2}\sigma\varepsilon^{-1}\mathrm{e}^{-\mathrm{i}\sigma\chi_0}\{1+\varepsilon^2(\mathrm{e}^{2\mathrm{i}\sigma\chi_0}-\mathrm{i}\sigma\chi_2)+O(\varepsilon^4)\}, \tag{40}$$

$$\cos(\theta-\chi) = \tfrac{1}{2}\varepsilon^{-1}\mathrm{e}^{\mathrm{i}\sigma(\theta-\chi_0)}\{1+\varepsilon^2(\mathrm{e}^{-2\mathrm{i}\sigma(\theta-\chi_0)}-\mathrm{i}\sigma\chi_2)+O(\varepsilon^4)\}, \tag{41}$$

$$D_0'(\varepsilon,\Omega_0,\chi) = \mathrm{i}(2\Omega_0\mathrm{e}^{-\mathrm{i}\sigma\chi_0}+5\sigma)+O(\varepsilon^2). \tag{42}$$

Hence, the leading-order approximation to Eq. (37) is

$$P^+(\chi) \simeq -\frac{\mathrm{i}\sigma\Omega_0\mathrm{e}^{\Psi}}{2(2\Omega_0+5\sigma\mathrm{e}^{\mathrm{i}\sigma\chi_0})}, \tag{43}$$

where the exponent Ψ is

$$\Psi = \tfrac{1}{2}\varepsilon\Omega_0 R\mathrm{e}^{\sigma\chi_{0\mathrm{i}}}\{-\sigma\sin(\theta-\chi_{0\mathrm{r}})+\mathrm{i}\cos(\theta-\chi_{0\mathrm{r}})\} \tag{44}$$

$$= \tfrac{1}{2}\varepsilon\Omega_0\mathrm{e}^{\sigma\chi_{0\mathrm{i}}}\{\sigma(X\sin\chi_{0\mathrm{r}}-Y\cos\chi_{0\mathrm{r}})+\mathrm{i}(X\cos\chi_{0\mathrm{r}}+Y\sin\chi_{0\mathrm{r}})\}. \tag{45}$$

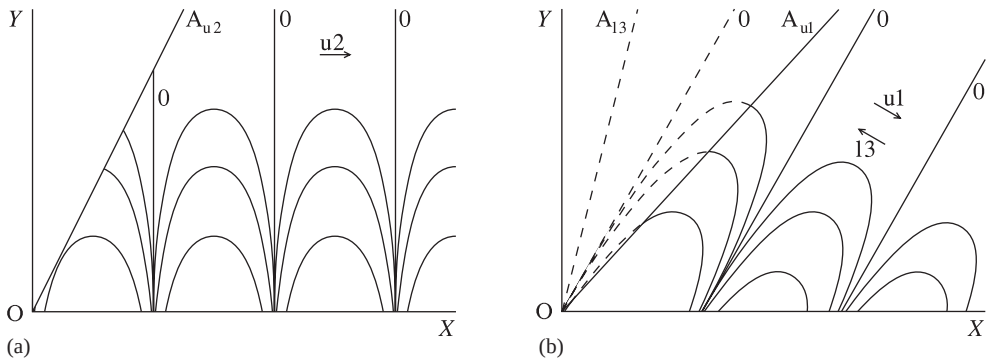

Fig. 5. Contours of the pressure field corresponding to (a) the surface wave P_{u2}, and (b) the evanescent waves P_{u1}, P_{l3}, corresponding to the poles $\chi_{u2}, \chi_{u1}, \chi_{l3}$. Contours for zero pressure are labelled 0. The cut-off lines are $OA_{u2}, OA_{u1}, OA_{l3}$, at angles $\theta_{u2}, \theta_{u1}, \theta_{l3}$ to the OX-axis, and the arrows $u2, u1, l3$ show the direction of phase propagation. In (b), the contours of P_{u1} are solid lines, and the contours of P_{l3} are these solid lines and their extensions as dashed lines, together with the straight dashed line labelled 0. Compare [12, p. 471, Fig. 5.3.8b].

Thus Eq. (43) represents an inhomogeneous plane wave with exponential decay of amplitude in the direction $(-\sigma \sin\chi_{0r}, \sigma\cos\chi_{0r})$, and phase propagation in the perpendicular direction $(\cos\chi_{0r}, \sin\chi_{0r})$; recall that $-\frac{1}{2}\pi \leqslant \chi_{0r} < \frac{3}{2}\pi$. Expression (35) for P_{u2} follows from Eqs. (43) and (45) with $\sigma = 1$ and $\chi_{0r} = 0$; the Heaviside term $H(\theta_{u2} - \theta)$ in Eq. (35) describes the fact, evident in Fig. 2, that in the deformation from C' to $C(0)$ the pole χ_{u2} is cut on when $\theta < \theta_{u2}$ and cut off when $\theta > \theta_{u2}$. Expression (36) for θ_{u2} follows from Eq. (34) with $\sigma = 1$, $\chi_{0r} = 0$, and $\chi_{2r} = 0$. The continuity of $P = P_{\text{poles}} + P_{\text{steep}}$, despite discontinuities in P_{poles} and P_{steep} individually, is discussed in Appendix D.

Contours of the surface-wave pressure field P_{u2} are shown in Fig. 5a. The cut-off angle θ_{u2} is $X\hat{O}A_{u2}$, and so contours are not shown to the left of the cut-off line OA_{u2}. From Eq. (35), the dimensionless wavelength of the surface wave is $4\pi/(\varepsilon\Omega_0 e^{\chi_{0i}})$, and the dimensionless penetration depth, i.e. the e-fold distance, is $2/(\varepsilon\Omega_0 e^{\chi_{0i}})$. These are each of order ε^{-1}, because Ω_0 is formally of order one in the expansion scheme. In dimensional variables, obtained from $X = k_c x$, $Y = k_c y$, and from the definitions of ε and Ω_0, the wavelength is $4\pi(\rho_0/\rho)(c_B/\omega)e^{-\chi_{0i}}$ and the penetration depth is $2(\rho_0/\rho)(c_B/\omega)e^{-\chi_{0i}}$. Here $e^{-\chi_{0i}}$ depends algebraically, not exponentially, on Ω_0, because Eq. (33a) is a polynomial in $e^{-\chi_{0i}}$, not in χ_{0i}. From the definition $\Omega_0 = (\omega h/c_B)/(\rho_0/\rho)^2$, it follows that the scaling law for the wavelength and the penetration depth is that each has the functional form $(\rho_0/\rho)(c_B/\omega)\text{fn}((\omega h/c_B)/(\rho_0/\rho)^2)$. The speed of sound c_0 is absent here, because at leading order the surface wave is incompressible.

4.2. Plate displacement in the surface wave

The plate displacement in the surface wave travelling to the right in Fig. 1 is given by the contribution of the pole χ_{u2} to the contour integral (26) for W, evaluated for $\theta = 0$, $R = X$. The contribution will be denoted W_{u2}; identical theory to that in Section 4.1 for the pressure field

shows that

$$W_{u2} = \frac{\mathrm{i}}{4\varepsilon^3} \frac{\mathrm{e}^{\chi_{0\mathrm{i}}}}{2\Omega_0 + 5\mathrm{e}^{-\chi_{0\mathrm{i}}}} \mathrm{e}^{\frac{1}{2}\mathrm{i}\varepsilon\Omega_0 R\mathrm{e}^{\chi_{0\mathrm{i}}}}. \tag{46}$$

Here $\chi_{0\mathrm{i}}$ is the same function of Ω_0 as in Section 4.1. The quantity W^+ corresponding to P^+ in Eq. (37) is

$$W^+ = \frac{1}{\varepsilon} \frac{\mathrm{e}^{\mathrm{i}\varepsilon^2\Omega_0 R\cos(\theta-\chi)}}{D_0'(\varepsilon,\Omega_0,\chi)} \sin^2\chi \quad (\theta = 0,\pi), \tag{47}$$

and the approximation for W^+ corresponding to that for P^+ is

$$W^+ \simeq \frac{\mathrm{i}}{4\varepsilon^3} \frac{\mathrm{e}^{-\mathrm{i}\sigma\chi_0}\mathrm{e}^{\Psi}}{2\Omega_0 + 5\sigma\mathrm{e}^{\mathrm{i}\sigma\chi_0}}. \tag{48}$$

Here Ψ is given by Eqs. (44)–(45), with $\theta = 0,\pi$ in Eq. (44), and with $Y = 0$ in Eq. (45). Expression (46) for W_{u2} follows from Eq. (48) with $\sigma = 1$ and $\chi_{0\mathrm{r}} = 0$.

In formulae for energy flow it is convenient to consider a slab of arbitrary width b in the z-direction, for example, consisting of the fluid and the plate within the region $0 \leqslant z \leqslant b$. Then formulae for rate of energy flow have dimensions energy per unit time, because the formulae contain a factor b. A standard calculation, based on Eq. (19) for p and on Eq. (35) for P_{u2}, shows that, in such a slab of width b, the fluid in the surface wave travelling to the right transports energy at a rate

$$\frac{1}{16\varepsilon} \frac{p_0^2 a^2 b}{\rho c_0 h} \frac{\Omega_0}{(2\Omega_0 + 5\mathrm{e}^{-\chi_{0\mathrm{i}}})^2} + O(\varepsilon). \tag{49}$$

A similar calculation, based on Eq. (25) for η and on Eq. (46) for W_{u2}, shows that the associated bending wave in the plate transports energy at a rate

$$\frac{1}{8\varepsilon} \frac{p_0^2 a^2 b}{\rho c_0 h} \frac{\Omega_0(\Omega_0\mathrm{e}^{\chi_{0\mathrm{i}}} + 2)}{(2\Omega_0 + 5\mathrm{e}^{-\chi_{0\mathrm{i}}})^2} + O(\varepsilon). \tag{50}$$

The total rate of energy flow in the surface wave travelling to the right is the sum of Eqs. (49) and (50), i.e.

$$\frac{1}{16\varepsilon} \frac{p_0^2 a^2 b}{\rho c_0 h} \frac{\Omega_0 \mathrm{e}^{\chi_{0\mathrm{i}}}}{2\Omega_0 + 5\mathrm{e}^{-\chi_{0\mathrm{i}}}} + O(\varepsilon). \tag{51}$$

The surface wave travelling to the left, corresponding to the pole $\chi_{\mathrm{l}4}$, gives identical values to Eqs. (49)–(51), so that the total rate of energy transported by the surface waves is twice (51).

The ratio of Eq. (49) to Eq. (50) is $2\Omega_0\mathrm{e}^{\chi_{0\mathrm{i}}} + 4$, or $8\Omega_0^{-3}\mathrm{e}^{-5\chi_{0\mathrm{i}}}$ by means of dispersion relation (33a). This ratio is of order one, i.e. in the surface wave comparable amounts of energy are transported by the fluid and the plate. When $\Omega_0 \to 0$, the dispersion relation shows that the ratio tends to one-quarter.

5. The acoustic field and the energy budget

5.1. Far acoustic field

The acoustic field propagating away from the origin in Fig. 1 is represented by the integral P_{steep} evaluated on the steepest-descent contour $C(\theta)$, as described in Section 2.3 and Appendix A. The far acoustic field, which begins at R of order ε^{-2}, is given by the saddle-point contribution P_{saddle} to P_{steep}. A calculation based on Eq. (24) or Eq. (A.4) shows that

$$P_{\text{saddle}} = \frac{\mathrm{e}^{-\pi \mathrm{i}/4}}{2^{1/2}\pi^{1/2}} \frac{\Omega_0 \sin\theta}{D_0(\varepsilon, \Omega_0, \theta)} \left(1 + \frac{1-\varepsilon^4\Omega_0^2}{\varepsilon R \sin\theta}\right) \frac{\mathrm{e}^{\mathrm{i}\varepsilon^2\Omega_0 R}}{(\Omega_0 R)^{1/2}}. \tag{52}$$

The second term in brackets is needed when $\sin\theta$ is of order $(\varepsilon R)^{-1}$ or smaller, i.e. $Y \leqslant O(\varepsilon^{-1})$, and describes the 'Lloyd's mirror' effect, which is that for grazing angles to the plate the acoustic field decays as $R^{-3/2}$, not $R^{-1/2}$. Since $D_0(\varepsilon, \Omega_0, \theta) = 1$ when $\theta = 0, \pi$, the grazing-angle limit of Eq. (52) is

$$P_{\text{saddle}} = \frac{\mathrm{e}^{-\pi \mathrm{i}/4}}{2^{1/2}\pi^{1/2}} \frac{\Omega_0^2}{\varepsilon} (1 - \varepsilon^4\Omega_0^2) \frac{\mathrm{e}^{\mathrm{i}\varepsilon^2\Omega_0 R}}{(\Omega_0 R)^{3/2}}. \tag{53}$$

The pressure field (53) produces a plate displacement given by the saddle-point contribution W_{saddle} to W_{steep}. A calculation based on Eq. (28) or Eq. (A.7) shows that

$$W_{\text{saddle}} = \frac{\mathrm{e}^{-\pi \mathrm{i}/4}}{2^{1/2}\pi^{1/2}} \frac{1-\varepsilon^4\Omega_0^2}{\varepsilon^4} \frac{\mathrm{e}^{\mathrm{i}\varepsilon^2\Omega_0 R}}{(\Omega_0 R)^{3/2}}. \tag{54}$$

In the derivation of Eqs. (52)–(54) the condition $\varepsilon \ll 1$ has not been used, and so the expressions remain valid up to ε of order one. When $\varepsilon \ll 1$, the terms $\varepsilon^4\Omega_0^2$ may be ignored.

5.2. Energy flow in the acoustic field

A calculation based on Eq. (19) for p and on Eq. (52) for P_{saddle} shows that in a slab of width b in the z-direction the acoustic field radiates energy at a rate

$$\frac{\varepsilon}{2\pi} \frac{p_0^2 a^2 b}{\rho c_0 h} \Omega_0 \int_0^{(1/2)\pi} \frac{\sin^2\chi \, \mathrm{d}\chi}{1 + \varepsilon^2\Omega_0^2(1 - \varepsilon^2\Omega_0^2\cos^4\chi)^2 \sin^2\chi}. \tag{55}$$

5.3. Energy budget

The forcing $f(t,x) = p_0\delta(x/a)\mathrm{e}^{\mathrm{i}\varepsilon^2\Omega_0 T}$ produces a power input E_{in}, in a width b in the z-direction, of

$$E_{\text{in}} = R\mathrm{e}\tfrac{1}{2}b \int_{-\infty}^{\infty} f\bar{\eta}_t \, \mathrm{d}x = \tfrac{1}{2}\varepsilon^2\Omega_0 \frac{p_0^2 a^2 b}{\rho c_0 h} W_{\mathrm{i}}|_{R=0}. \tag{56}$$

Here $W_{\mathrm{i}}|_{R=0}$ is the imaginary part of Eq. (26), evaluated at $R=0$. If the contour C' in Eq. (26) is deformed on to the rectilinear path from $\frac{1}{2}\pi - \mathrm{i}\infty$ to $-\frac{1}{2}\pi + \mathrm{i}\infty$ via $\frac{1}{2}\pi$ and $-\frac{1}{2}\pi$, the total contribution from the vertical sections vanishes. The symmetry in χ then gives

$$E_{\mathrm{in}} = \frac{\varepsilon}{2\pi}\frac{p_0^2 a^2 b}{\rho c_0 h}\Omega_0 \int_0^{(1/2)\pi} \frac{\sin^2\chi \,\mathrm{d}\chi}{1+\varepsilon^2\Omega_0^2(1-\varepsilon^2\Omega_0^2\cos^4\chi)^2\sin^2\chi} + \frac{1}{8\varepsilon}\frac{p_0^2 a^2 b}{\rho c_0 h}\frac{\Omega_0 \mathrm{e}^{\chi_{0\mathrm{i}}}}{2\Omega_0 + 5\mathrm{e}^{-\chi_{0\mathrm{i}}}} + \cdots . \tag{57}$$

The first term here is obtained by combining the integrals from $-\frac{1}{2}\pi$ to 0 and from 0 to $\frac{1}{2}\pi$; the second term, to be evaluated at χ_{u2}, is all that remains of the pole contributions, because the contributions from χ_{u1} and χ_{l3} cancel out. The first term on the right of Eq. (57) is the rate of acoustic energy radiation, Eq. (55), and the second term is the total rate of energy transport by the surface wave to the left and the surface wave to the right, i.e. twice Eq. (51). Thus Eq. (57) is the energy-budget relation, equating the power input to the power output. The ratio of the acoustic radiation to the surface-wave energy transport is of order ε^2.

6. The inner near field

The inner near field extends from the origin $R=0$ out to R of order ε^{-1}. In this region the evanescent waves, represented by the poles $\chi_{u1}, \chi_{u3}, \chi_{l3}, \chi_{l5}$, have the same order of magnitude as the surface waves and of the steepest-descent contribution to the field. Thus the inner near field requires for its description all six important poles, namely $\chi_{u1}, \chi_{u2}, \chi_{u3}, \chi_{l3}, \chi_{l4}, \chi_{l5}$, and also the integral P_{steep} or W_{steep}; no further simplification or approximation is available. The evanescent waves P_{u1} and P_{l3}, to the right of the origin, are shown in Fig. 5b. Simple expressions for P_{u1} and P_{l3} are obtained from Eqs. (43)–(45) evaluated at χ_{u1} and χ_{l3}; for example, $P_{u1} = H(\theta_{u1} - \theta)P^+_{u1}$. The field P_{l3} differs from P_{u1} only in that the phase propagates in the opposite direction and the cut-off line OA_{l3} is slightly above OA_{u1}. Below OA_{u1}, the sum of the fields P_{u1} and P_{l3} is the standing wave $2\mathrm{Re}\,(P_{u1})$, i.e.

$$P_{u1} + P_{l3} \simeq \frac{\Omega_0}{|2\Omega_0 + 5\mathrm{e}^{\mathrm{i}\chi_0}|}\exp\{-\tfrac{1}{2}\varepsilon\Omega_0 R\mathrm{e}^{\chi_{0\mathrm{i}}}\sin(\theta - \chi_{0\mathrm{r}})\} \times \cos\{-\alpha_0 + \tfrac{1}{2}\varepsilon\Omega_0 R\mathrm{e}^{\chi_{0\mathrm{i}}}\cos(\theta - \chi_{0\mathrm{r}})\}, \tag{58}$$

in which χ_0 is evaluated at χ_{u1}, and α_0 is the phase of $2\Omega_0 + 5\mathrm{e}^{\mathrm{i}\chi_0}$. Since Ω_0 is formally of order one, the exponential term in Eq. (58) shows that the evanescent waves are negligible when εR is greater than order one, i.e. when R is greater than order ε^{-1}; this fact defines the inner near field as extending to R of order ε^{-1}.

Similar remarks apply to the plate displacement. The evanescent waves to the right of the origin are represented by poles χ_{u1} and χ_{l3}, the sum of the corresponding displacements being $W_{u1} + W_{l3} = H(\theta_{u1})W^+_{u1} + W^+_{l3}$, by Eqs. (47)–(48). When $\theta_{u1} > 0$, the sum is $2\,\mathrm{Re}(W^+_{u1})$.

7. Conclusion

It has been seen that the forced vibration of an elastic plate under significant fluid loading admits a simple description by means of expansions in the intrinsic fluid-loading parameter $\varepsilon = (\rho_0/\rho)/(c_0/c_B)$. The coefficients in these expansions are functions of the reduced frequency $\Omega_0 = (\omega h/c_B)/(\rho_0/\rho_B)^2$. In the dimensionless variables used, the wavelength of the radiated sound in the water is of order ε^{-2}, and the principal scaling laws obtained, for Ω_0 of order one, are as follows. The near acoustic field, of radius of order ε^{-2}, contains within it a much smaller region, the inner near field, of radius of order ε^{-1}, strongly influenced by the plate. The surface wave propagating next to the plate has wavelength of order ε^{-1}, and the penetration distance of this wave into the fluid is also of order ε^{-1}. The radiated acoustic power is of order ε. The surface wave transports fluid kinetic energy at a rate of order ε^{-1}, plate bending-wave energy also at a rate of order ε^{-1}, and fluid potential energy at a negligible rate. Thus the total rate of energy transport in the surface wave, of order ε^{-1}, is greater than that in the directly radiated acoustic field by a factor of order ε^{-2}. For all of the above quantities, the paper also gives the coefficient of the stated power of ε as a function of Ω_0. Thus the paper gives simple expressions for all the important physical quantities relating to the forced vibration of the plate. The expressions are valid not only for Ω_0 of order one, but also for Ω_0 arbitrarily small, i.e. for heavy fluid loading, because in all the expansions the limit $\Omega_0 \to 0$ is uniform. Comparison of the exact solutions of the dispersion relation with the solutions obtained from the dominant balance show that the expressions are accurate up to a forcing frequency of about half the coincidence frequency. Thus, the range of validity is approximately $\Omega \leqslant \frac{1}{2}$, or $\Omega_0 \leqslant \frac{1}{2}\varepsilon^{-2}$. Since $\varepsilon = 0.134$ for steel in water, this gives approximately $\Omega_0 \leqslant 28$. That this range of validity is far larger than would be expected from a literal interpretation of 'Ω_0 is of order one' is no surprise: it is the normal situation for an expansion based on a significant scaling. The results in this paper provide a foundation for scaling-based analyses of further effects, e.g. nonlinearity [14], and scattering at the edge of the plate, at inhomogeneities, and at supports.

Acknowledgements

This work has been supported by a Joint Project Grant from the Royal Society.

Appendix A. Numerical integration

In contour integrals with respect to χ, a useful alternative variable of integration is a quantity s satisfying

$$\cos(\theta - \chi) = 1 + \tfrac{1}{2}\mathrm{i}s^2. \tag{A.1}$$

Then

$$\chi = \theta - \mathrm{sgn}(s)\cos^{-1}(1 + \tfrac{1}{2}\mathrm{i}s^2), \quad \sin(\theta - \chi) = \mathrm{e}^{-\pi\mathrm{i}/4}s(1 + \tfrac{1}{4}\mathrm{i}s^2)^{1/2}, \tag{A.2a, b}$$

$$\mathrm{d}\chi = \frac{\mathrm{i}s\,\mathrm{d}s}{\sin(\theta-\chi)} = \mathrm{e}^{3\pi\mathrm{i}/4}(1+\tfrac{1}{4}\mathrm{i}s^2)^{-1/2}\,\mathrm{d}s, \tag{A.3}$$

so that

$$P_{\text{steep}} = -\frac{\mathrm{i}\varepsilon\Omega_0}{2\pi}\mathrm{e}^{\mathrm{i}\varepsilon^2\Omega_0 R}\int_{-\infty}^{\infty}\frac{\mathrm{e}^{-\frac{1}{2}\varepsilon^2\Omega_0 R s^2}}{D_0(\varepsilon,\Omega_0,\chi)}\frac{\sin\chi}{\sin(\theta-\chi)}s\,\mathrm{d}s \tag{A.4}$$

in which χ and $\sin(\theta-\chi)$ are the functions of s given by (Eq. A.2). For $\theta=0$, i.e. along the plate, (Eq. A.4) gives

$$P_{\text{steep}} = \frac{\mathrm{i}\varepsilon\Omega_0}{2\pi}\mathrm{e}^{\mathrm{i}\varepsilon^2\Omega_0 R}\int_{-\infty}^{\infty}\frac{\mathrm{e}^{-\frac{1}{2}\varepsilon^2\Omega_0 R s^2}s\,\mathrm{d}s}{1+\mathrm{e}^{\pi\mathrm{i}/4}\varepsilon\Omega_0 s(1+\frac{1}{4}\mathrm{i}s^2)^{1/2}\{1-\varepsilon^4\Omega_0^2(1+\frac{1}{2}\mathrm{i}s^2)^4\}}, \tag{A.5}$$

and for $\theta=\frac{1}{2}\pi$, i.e. at right angles to the plate, it gives

$$P_{\text{steep}} = \frac{\mathrm{e}^{-\pi\mathrm{i}/4}\varepsilon\Omega_0}{2\pi}\mathrm{e}^{\mathrm{i}\varepsilon^2\Omega_0 R}\int_{-\infty}^{\infty}\frac{\mathrm{e}^{-\frac{1}{2}\varepsilon^2\Omega_0 R s^2}(1+\frac{1}{2}\mathrm{i}s^2)(1+\frac{1}{4}\mathrm{i}s^2)^{-1/2}\,\mathrm{d}s}{1-\mathrm{i}\varepsilon\Omega_0(1+\frac{1}{2}\mathrm{i}s^2)\{1+\varepsilon^4\Omega_0^2 s^4(1+\frac{1}{4}\mathrm{i}s^2)^2\}}. \tag{A.6}$$

Integrals (A.4)–(A.6) are well adapted to numerical integration. In addition, the 'window function' $\mathrm{e}^{-\frac{1}{2}\varepsilon^2\Omega_0 R s^2}$ allows the important range of s in the integrals to be determined, so that the order of magnitude of the integrals may be estimated analytically as a power of ε for different ranges of R. The results are shown schematically in Fig. 6a,b. The significant locations are $R\sim\varepsilon^{-1}$ and $R\sim\varepsilon^{-2}$, and the orders of magnitude match smoothly. The region $R>\varepsilon^{-2}$ is the acoustic far field; the region $\varepsilon^{-1}<R<\varepsilon^{-2}$ is the acoustic near field; and the region $R<\varepsilon^{-1}$ is the inner near field. Fig. 6 is invaluable in comparing the orders of magnitude of P_{steep} and the individual contributions to P_{poles}.

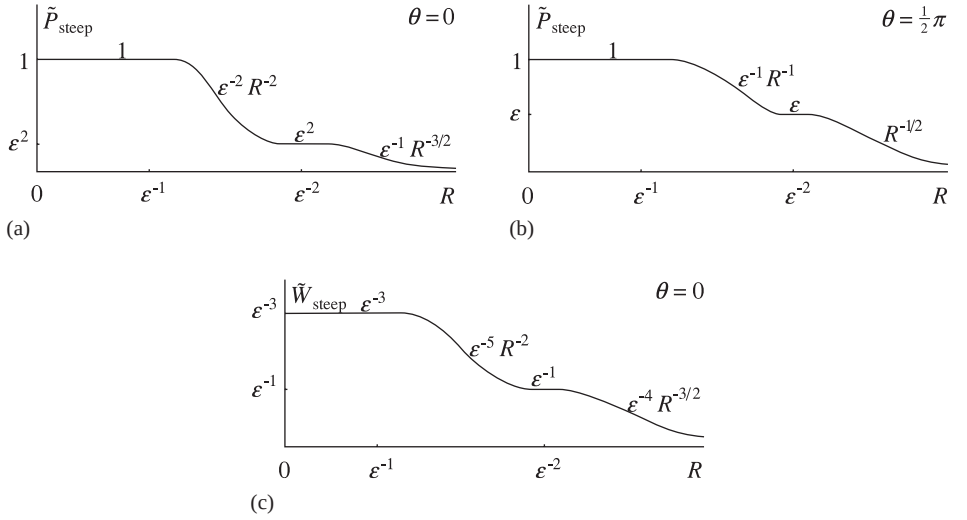

Fig. 6. (a, b) Orders of magnitude, as a function of R, of real or imaginary part $\tilde{P}_{\text{steep}}$ of P_{steep} defined by integrals (A.4)–(A.6) when $\theta=0,\frac{1}{2}\pi$. (c) As (a), (b), but for the real or imaginary part $\tilde{W}_{\text{steep}}$ of W_{steep} defined by the integral (A.7) for $\theta=0$. For a fluid-loaded membrane rather than a plate, compare [13, Fig. 2].

Inspection of the order of magnitude of P_{steep} as a function of R in Fig. 6b indicates a range of R from ε^{-1} to ε^{-2} in which P_{steep} decays as R^{-1}. This range of R is the acoustic near field, and P_{steep} in this range gives the acoustic near-field pressure. The acoustic near-field region is clearly identifiable in Fig. 1, where it lies between $R \simeq 10$ and 100. The length scale of variation of pole contributions is ε^{-1}, and that of steepest-descent contributions is ε^{-2}, except that when R is of order ε^{-1} or less, i.e. when R is in the inner near field, the length-scale of variation of steepest-descent contributions is of order ε^{-1}.

When $\theta = 0$, the steepest-descent integral for the plate displacement, analogous to Eq. (A.5) for the acoustic pressure, is

$$W_{\text{steep}} = \frac{\mathrm{e}^{-\pi \mathrm{i}/4}}{2\pi\varepsilon} \mathrm{e}^{\mathrm{i}\varepsilon^2\Omega_0 R} \int_{-\infty}^{\infty} \frac{\mathrm{e}^{-\frac{1}{2}\varepsilon^2\Omega_0 R s^2} s^2 (1+\frac{1}{4}\mathrm{i}s^2)^{1/2}\,\mathrm{d}s}{1+\mathrm{e}^{\pi\mathrm{i}/4}\varepsilon\Omega_0 s(1+\frac{1}{4}\mathrm{i}s^2)^{1/2}\{1-\varepsilon^4\Omega_0^2(1+\frac{1}{2}\mathrm{i}s^2)^4\}}. \tag{A.7}$$

The order of magnitude of Eq. (A.7) as a function of R is shown schematically in Fig. 6c.

Appendix B. The heavy fluid loading limit

Although Eq. (31) has been obtained on the assumption that Ω_0 is of order one, the heavy fluid loading limit $\Omega_0 \to 0$ is regular, so that Eqs. (30a,b), (31) remain valid when $\Omega_0 \to 0$ and give correct results for $\Omega_0 \ll \varepsilon^2$, i.e. for heavy fluid loading. Thus in Eq. (31a) assume that $\Omega_0 \ll 1$ and $K_0 \sim \Omega_0^q$. A dominant balance occurs only for $q = \frac{2}{5}$, in which case the term $-\Omega_0^2 K_0$ is negligible and Eq. (31a) reduces to the heavy fluid loading approximation $K_0^5 \simeq \pm\Omega_0^2$. As this equation can be solved at once for all its complex roots K_0, it has been used in earlier investigations [1,2,5]; but the range of frequencies for which it gives accurate results is narrower than for Eq. (31a), because it does not balance the maximum number of terms at leading order, i.e. does not correspond to a significant limit. The non-significant heavy fluid loading approximation $K_0^5 \simeq \pm\Omega_0^2$, valid when $\Omega_0 \ll 1$, i.e. $K_0 \ll 1$, is equivalent in unscaled variables to $K^5 \simeq \varepsilon\Omega^2$, valid when $\Omega \ll \varepsilon^2$, i.e $K \ll \varepsilon$. All results obtainable from this non-significant heavy fluid loading approximation are recovered by taking the trivial regular limit $\Omega_0 \to 0$ in results for significant fluid loading; but the non-significant approximation does not determine what happens when Ω_0 is of order one, i.e. when the fluid loading is significant.

Appendix C. Symmetry of the dispersion relation

The symmetry of the dispersion relation $D(\varepsilon, \Omega, \chi) = 0$, or equivalently $D_0(\varepsilon, \Omega_0, \chi) = 0$, is such that, for real Ω or Ω_0, if χ is a root then (with a bar denoting complex conjugate) so are $-\bar{\chi}$, $\bar{\chi} + \pi$, and $-\chi + \pi$. Thus, the roots form groups of four, except that roots with real parts which are multiples of π form groups of two. The corresponding symmetry in expansion (32) is that if (σ, χ_0, χ_2) gives a root then so do $(\sigma, -\bar{\chi}_0, -\bar{\chi}_2)$, $(-\sigma, \bar{\chi}_0 + \pi, \bar{\chi}_2)$, and $(-\sigma, -\chi_0 + \pi, -\chi_2)$. The groups in Fig. 2 are $(\chi_{u1}, \chi_{u3}, \chi_{l3}, \chi_{l5})$, $(\chi_{u4}, \chi_{u5}, \chi_{l1}, \chi_{l2})$, and (χ_{u2}, χ_{l4}), in which multiples of 2π have been added or subtracted to return the values of χ to the fundamental strip $-\frac{1}{2}\pi \leqslant \chi_{\mathrm{r}} < \frac{3}{2}\pi$.

Appendix D. Cancellation of discontinuities

In the decomposition $P = P_{\text{poles}} + P_{\text{steep}}$ the terms P_{poles} and P_{steep} are each discontinuous at $\theta = \theta_{u1}, \ldots, \theta_{l5}$, but the total P is continuous, i.e. the discontinuities are equal and opposite and cancel out. Across the cut-off line OA_{u2} in Fig. 5a, the discontinuity between zero pressure and the surface-wave pressure is thus exactly matched by an equal and opposite discontinuity in the contour integral along $C(\theta)$ as θ crosses the value θ_{u2}, at which a pole lies exactly on the contour $C(\theta)$. Numerically this discontinuity is often smaller in magnitude than one might expect. For example, Eq. (43) shows that the discontinuity ΔP_{u2} in (35) at $\theta = \theta_{u2}$ is

$$\Delta P_{u2} \simeq -\frac{\mathrm{i}\Omega_0 \mathrm{e}^{-\frac{1}{2}\varepsilon\Omega_0 R\mathrm{e}^{\chi_{0\mathrm{i}}} + \mathrm{i}\varepsilon^2\Omega_0 R}}{2(2\Omega_0 + 5\mathrm{e}^{-\chi_{0\mathrm{i}}})}. \tag{D.1}$$

Here the phase variation is represented by $\mathrm{e}^{\mathrm{i}\varepsilon^2\Omega_0 R}$, and the previous combination εR has been replaced by $\varepsilon^2 R$, i.e. the phase length-scale has increased from ε^{-1} to ε^{-2}. The explanation, from Fig. 5a, is that the cut-off line OA_{u2} is inclined at only a small angle, of order ε, to the direction of no phase variation, i.e. OY. The significance of this phase variation along the cut-off line OA_{u2} is that the phase term in P_{steep} is also represented by $\mathrm{e}^{\mathrm{i}\varepsilon^2\Omega_0 R}$; i.e. the cut-off line OA_{u2} is obligingly positioned to make the transition across it as 'tame' as possible.

References

[1] D.G. Crighton, Fluid-loading interaction with vibrating surfaces, in: D.G. Crighton, A.P. Dowling, J.E. Ffowcs Williams, M. Heckl, F.G. Leppington (Eds.), *Modern Methods in Analytical Acoustics*, Springer, London, 1992, pp. 510–523.

[2] D.G. Crighton, D. Innes, The modes, resonances, and forced response of elastic structures under heavy fluid loading, *Philosophical Transactions of the Royal Society of London A* 312 (1984) 295–341.

[3] L.Ya. Gutin, Sound radiation from an infinite plate excited by a normal point force, *Soviet Physics—Acoustics* 10 (1965) 369–375.

[4] P.R. Nayak, Line admittance of infinite isotropic fluid-loaded plates, *Journal of the Acoustic Society of America* 47 (1970) 191–201.

[5] D.G. Crighton, The 1988 Rayleigh medal lecture: fluid loading—the interaction between sound and vibration, *Journal of Sound and Vibration* 133 (1989) 1–27.

[6] M.C. Junger, D. Feit, *Sound, Structures, and their Interaction*, 2nd edn, MIT Press, Cambridge, MA, 1986.

[7] M.S. Howe, *Acoustics of Fluid–Structure Interactions*, Cambridge University Press, Cambridge, 1998.

[8] G.F. Carrier, M. Krook, C.E. Pearson, *Functions of a Complex Variable: Theory and Technique*, Hod, New York, 1983.

[9] P.M. Morse, H. Feshbach, *Methods of Theoretical Physics—Part 1*, McGraw-Hill, New York, 1953.

[10] C.J. Chapman, High-speed leading-edge noise, *Proceedings of the Royal Society of London A* 459 (2003) 2131–2151.

[11] D.G. Crighton, Approximations to the admittances and free wavenumbers of fluid-loaded panels, *Journal of Sound and Vibration* 68 (1980) 15–33.

[12] L.B. Felsen, N. Marcuvitz, *Radiation and Scattering of Waves*, Oxford University Press, Oxford, 1994.

[13] D.G. Crighton, The Green function of an infinite, fluid loaded membrane, *Journal of Sound and Vibration* 86 (1983) 411–433.

[14] S.V. Sorokin, C.J. Chapman, Asymptotic analysis of non-linear vibration of an elastic plate under heavy fluid loading, *Journal of Sound and Vibration*, in press; doi:10.1016/j.jsv.2004.08.003.